



Article

# Study of Cretaceous Provenance Tracing and Sedimentary Patterns in the Western Qiantang Sag, East China Sea Shelf Basin

Kailong Feng <sup>1,2,3</sup> , Weilin Zhu <sup>1,3</sup>, Xiaowei Fu <sup>1,3</sup>, Kai Zhong <sup>1,3,\*</sup>, Shijie Zhao <sup>1,3</sup>, Weizhen Chen <sup>2</sup>, Zengyuan Zhou <sup>1,3</sup>  and Lichen Hu <sup>1,3</sup>

<sup>1</sup> School of Ocean and Earth Science, Tongji University, Shanghai 200092, China;

fengkailong@tongji.edu.cn (K.F.); zhuwl@tongji.edu.cn (W.Z.); fu\_xiaowei@tongji.edu.cn (X.F.)

<sup>2</sup> Key Laboratory of Deep-Time Geography and Environment Reconstruction and Applications of Ministry of Natural Resources, Chengdu University of Technology, Chengdu 610059, China; cwz@stu.cdut.edu.cn

<sup>3</sup> Center for Marine Resources, Tongji University, Shanghai 200092, China

\* Correspondence: zhongkai@tongji.edu.cn

**Abstract:** The Qiantang Sag, as one of the East China Sea Shelf Basin's sags with thick residual Mesozoic strata, has long lacked comprehensive foundational sedimentary research, significantly impeding the understanding of the region's resource potential and geological history. This study focuses on the Cretaceous strata of the Qiantang Sag, proposing a multi-phase sedimentary model for the Cretaceous Period. Through detailed analysis of the regional geological structure and sedimentary strata, this study unveils the complex sedimentary processes experienced by the Qiantang Sag during the Cretaceous. Utilizing drilling and core data combined with seismic geological interpretation, this study identifies that the western part of the Qiantang Sag predominantly developed alluvial fan and braided river deposits in an arid to semi-arid environment during the Cretaceous. Detrital zircon U-Pb dating analysis provides key information on the provenance areas and sedimentation ages, indicating that the Zhe-Min Uplift was the primary source region for the Qiantang Sag during the Cretaceous. Integrating vertical sedimentary sequences with provenance analysis, this study proposes sedimentary models and reconstructs the paleo-depositional evolution of the Qiantang Sag across different geological periods. During the Early Cretaceous Yushan Period, the region was influenced by intense volcanic activity, while also developing alluvial fan deposits in an arid environment. The Late Cretaceous Minjiang Period was characterized by semi-arid alluvial fan and braided river deposits. In contrast, the subsequent Shimentan Period saw the development of similar deposits, with the possible addition of seasonal lake deposits.

**Keywords:** Cretaceous; sedimentary models; provenance analysis; detrital zircon; East China Sea Shelf Basin; Qiantang Sag



**Citation:** Feng, K.; Zhu, W.; Fu, X.; Zhong, K.; Zhao, S.; Chen, W.; Zhou, Z.; Hu, L. Study of Cretaceous Provenance Tracing and Sedimentary Patterns in the Western Qiantang Sag, East China Sea Shelf Basin. *J. Mar. Sci. Eng.* **2024**, *12*, 474. <https://doi.org/10.3390/jmse12030474>

Academic Editor: Assimina Antonarakou

Received: 1 January 2024

Revised: 7 March 2024

Accepted: 8 March 2024

Published: 10 March 2024



**Copyright:** © 2024 by the authors. Licensee MDPI, Basel, Switzerland. This article is an open access article distributed under the terms and conditions of the Creative Commons Attribution (CC BY) license (<https://creativecommons.org/licenses/by/4.0/>).

## 1. Introduction

The East China Sea (ECS) Shelf Basin, located in the East China Sea waters, is a large oil- and gas-bearing basin formed by the superposition of Mesozoic–Cenozoic sedimentary layers [1–5]. Over the past half-century of oil and gas exploration, more than ten commercial oil and gas fields have been discovered in this basin [6]. However, compared to the vast scale of this sedimentary basin, such oil and gas discoveries seem relatively insufficient [6–9]. All current oil and gas discoveries originate from Cenozoic strata, and researchers have divergent views on the distribution characteristics and oil and gas resource potential of the Mesozoic strata [5–22].

Despite the ECS Shelf Basin retaining abundant Mesozoic strata, understanding of its distribution characteristics and resource potential remains limited. This limitation stems partly from scarce basic data, such as little drilling into the Mesozoic layers and poor quality of mid-to-deep seismic data, hindering extensive studies of sedimentary characteristics [4,23–25]. Moreover, the ECS Shelf Basin has been under the influence of the

subduction system since the Mesozoic era, experiencing the subduction of the Paleo-Pacific, Pacific, and Philippine plates, making it the most prolonged and complex subduction-affected region in China's offshore areas [22,25–33]. This history of multiple tectonic shifts and superimposed prototypical basins adds to the complexity of understanding the sedimentary evolution of the ECS Shelf Basin.

With the intensification of exploration of Mesozoic oil and gas resources, numerous researchers have begun to focus on the study of Mesozoic strata [3,4,6,13,15,20,21,23–25,29,32]. Current research mainly concentrates on the Fuzhou Sag in the southern part of the ECS Shelf Basin, while the study of Mesozoic sedimentation in the Qiantang Sag, located in the central-southern part of the ECS Shelf Basin, is relatively scarce due to the extensive development of 'red beds'. As a significant component of the ECS Shelf Basin, the Qiantang Sag retains substantial Mesozoic sedimentary strata [6,34–37], potentially rich in geological records related to plate subduction. This makes the study of its provenance and sedimentary evolution of great significance for a deeper understanding of the subduction history of the West Pacific margin and the development of the basin. Therefore, research on the characteristics of its source and sedimentary evolution is highly necessary.

Despite the lack of attention from researchers and energy companies, research on the Qiantang Depression has still made some progress since the beginning of the 21st century. Gao Dezhang et al., based on the 1:200,000 gravity and magnetic results of the Qiantang area in the East China Sea, used techniques such as wavelet multi-scale decomposition and full magnetic latitude tilt angle polar conversion to determine the presence of Mesozoic strata in the Qiantang Sag area, and speculated the possible existence of Paleozoic strata [34]. Zhao Lei and Xia Qingqing, through their study of seismic profile stratigraphic frameworks, believe that the Qiantang Sag is a structural unit with Mesozoic–Cenozoic sedimentary infill, where the Cenozoic sedimentation is thin and of relatively small scale, and it has a distinct double fault structure [35,36]. Jiang Yiming et al., in their research on the edge structure of the Xihu Sag, found that the sedimentary strata of the Qiantang Sag can be traced in the seismic profile to the Pinghu Main Fault of the Xihu Sag, but due to limitations in seismic data quality, the contact relationship is difficult to confirm [37]. Zhong Kai et al., through a comprehensive study combining seismic profiles and drilling data with borehole seismic calibration, pointed out that Mesozoic strata are extensively eroded in the central part of the entire ECS Shelf Basin. Simultaneously, it was discovered that there are multiple syncline structures, characteristics of strong stratigraphic folds, and that the Mesozoic strata are mainly concentrated in the Qiantang Sag [6].

It should be emphasized that studies related to the Qiantang Sag are often mentioned as a part of the overall research on the ECS Shelf Basin [6,35,36]. Some scholars have also conducted certain studies on the Qiantang Sag while researching its adjacent areas [37]. However, research specifically focused on the Qiantang Sag itself is relatively limited, and studies that primarily focus on its Mesozoic sedimentary strata are even rarer.

This study comprehensively collected data related to the Qiantang Sag and for the first time conducted a detailed stratigraphic and sedimentary sequence analysis of the Cretaceous strata in the Qiantang Sag's A-1 borehole. By integrating stratigraphic identification from seismic profiles and borehole seismic correlation, a deep analysis of the structure and stratigraphic distribution of the Qiantang Sag was performed. Following the identification of the vertical sedimentary facies of the Cretaceous strata, a detrital zircon provenance study was conducted, revealing the main source directions and types, thus constructing the sedimentary evolution model of the Qiantang Sag during the Cretaceous Period.

## 2. Geological Setting

The ECS Shelf Basin, located on the southeastern margin of the Eurasian Plate and at the convergence zone of the Pacific and Eurasian Plates [2,38,39], is closely linked to the evolution of the subduction of the Paleo-Pacific Plate and the Pacific Plate, forming a key component of the West Pacific continental margin system [40–47]. In recent years, the academic community has conducted numerous studies on the tectonic background and

sedimentary characteristics of the ECS Shelf Basin, making it one of the most extensively studied basins in China's offshore areas.

The ECS Shelf Basin is the largest Mesozoic and Cenozoic superimposed basin in China's offshore area, covering an area of 267,000 km<sup>2</sup>, approximately 1100 km long from north to south, and 325 to 500 km wide from east to west [2,3]. The basin mainly extends in a northeast direction, bordered by the structural units of the Ryukyu Uplift to the east-southeast and the Zhe-Min Uplift to the west-northwest. (Figure 1) [9,23,46].

Structurally, it can be divided into three primary tectonic units and seven secondary tectonic units, including the western depression belt (Yangtze Depression, Taibei Depression, and Pengjia Island Depression), the central uplift belt (Hupijiao Uplift, etc.), and the eastern depression belt (Zhedong Depression) (Figure 1) [6,9].

The main tertiary level units include the Fujiang Sag, Xihu Sag, and Diaobei Sag in the northern, central, and southern parts of the Zhedong Depression; the Qiantang Sag, Jiaojiang Sag, Lishui Sag, Fuzhou Sag, and Yandang Uplift in the Taibei Depression; and the Kunshan Sag, Jinshan North Sag, Changshu Low Uplift, and Jinshan South Sag in the Yangtze Depression (Figure 1) [6].

The Qiantang Sag, analyzed in this study, is positioned within the Taibei Depression, part of the western depression belt. It lies southwest of the Haijiao Uplift. To the south, the sag is bounded by a northeast-dipping normal fault, marking the boundary with the Yushan Eastern Uplift. Northward, it adjoins the Haijiao Uplift, transitioning through a slope that rises westward. The sag's western proximity is to the Zhe-Min Uplift, and on the east, it intermittently connects to the Xihu Sag via a high saddle area, indicating an intermittent transition zone where the strata are not continuously traceable across the two depressions. Additionally, the southwest portion of the Qiantang Sag transitions into the Oujiang Sag through a distinct low saddle area [6,48].

Regarding the Mesozoic basin type of various sags within the East China Sea Shelf Basin, scholarly opinions are diverse. Some sags are considered forearc basins, while others are regarded as foreland basins. However, for those depressions adjacent to the Zhe-Min Uplift, such as the Lishui Sag and Qiantang Sag, researchers generally classify them as rift basins [6,35,36,48]. They exhibit rift basin characteristics similar to several Mesozoic basins along the coastal region of present-day South China (e.g., the Jinqu Basin, Linhai Basin). This similarity is unsurprising as the East China Sea Shelf Basin is closely adjacent to South China. Scholars suggest that the basement of the current East China Sea Shelf Basin is naturally extended from South China [44,49], which underwent significant geological and environmental changes during the Cretaceous period, as evidenced by the widespread distribution of red beds. Characterized by distinctive red sedimentary rocks, these Cretaceous red beds cover numerous sedimentary basins in South China and adjacent areas, indicating the extensive terrestrial depositional environment of the South China region during the Cretaceous period [50–52]. These basins often underwent rapid sedimentary filling, forming sedimentary rock sequences of red beds with thicknesses reaching several kilometers, mainly composed of red mudstone, sandstone, and conglomerate. Current research also indicates that the Cretaceous red beds developed in the coastal areas of Eastern South China, in the Zhejiang (Zhe)-Fujian (Min) region, primarily formed in subtropical–tropical arid to semi-arid depositional environments [53–55]. As a basin adjacent to the Zhejiang–Fujian region, the Qiantang Sag also developed similar red bed sedimentation during the Cretaceous.

However, unlike the less studied Qiantang Sag, the Lishui Sag has been more thoroughly researched. The Lishui Sag developed extensive red mudstone strata in the Upper Cretaceous and displayed seismic profiles interpreted as showing characteristics of alluvial fans and volcanoclastic facies [56]. This can be mutually corroborated with the continental red beds of the basins along the coast of South China, providing inferential evidence for the Qiantang Sag, which is closely adjacent to the Zhe-Min Uplift and Lishui Sag.

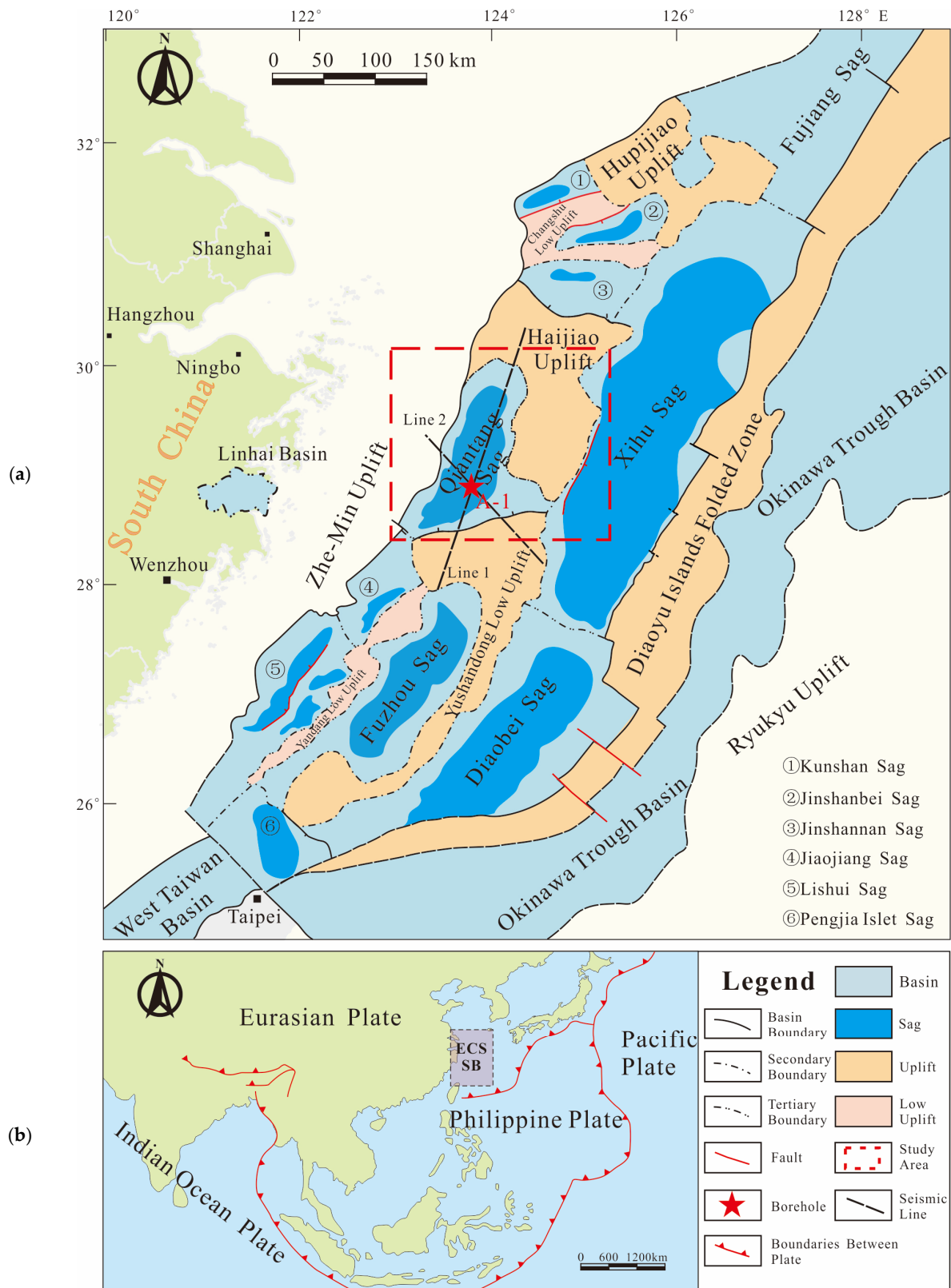


**Figure 1.** (a) Tectonic sketch of the East China Sea Shelf Basin and the location of the Qiantang Sag (modified from References [2,45]). (b) The tectonic location of the East China Sea Shelf Basin (modified from References [2,56]).

Moreover, limited by the quality of seismic data in the Qiantang Sag, it is difficult to identify the seismic facies of the Mesozoic strata down to the second level. In this area, there is only one exploration borehole available for stratigraphic and sedimentary constraints, and the vertical sedimentary sequence of this sole borehole has not been studied in detail. Additionally, due to the difficulty in obtaining samples, no detrital zircon provenance analysis has been conducted for the Mesozoic basin of the Qiantang Sag. Overall, basic sedimentological research on the Qiantang Sag is significantly lacking.

### 3. Materials and Methods

#### 3.1. Data and Materials

Borehole A-1 is situated in the central-southern part of the Qiantang Sag, and currently, it is the sole available borehole in the Qiantang Sag. CNOOC and Sinopec provided the stratigraphic division scheme for each section within this borehole and supplied basic lithological characteristics data of the Cretaceous strata. CNOOC and Sinopec also supplied two seismic lines that pass through borehole A-1 from different directions.

Observations of the Cretaceous intervals in borehole A-1 involved core examination, with a hundred high-resolution photographs taken, covering both continuous drilling core segments and focused shots of particularly typical individual cores. A total of 10 samples were collected, of which 7 samples were used to prepare microscopic thin sections, and the other three samples were used for detrital zircon provenance analysis.

#### 3.2. Methods

##### 3.2.1. Seismic Data Study and Application

The analysis of seismic data was carried out at the Center for Marine Resources, Tongji University. Based on the stratigraphic division scheme for the A-1 borehole provided by Sinopec, key stratigraphic reflection interfaces on the seismic lines passing through borehole A-1 were identified and marked. By locating these markers, the extension of strata could be tracked. Utilizing borehole seismic integration study [57], the distribution of Cretaceous strata in various directions across the western part of the Qiantang Depression was revealed.

##### 3.2.2. Preparation and Observation of Microscopic Thin Sections

The pretreatment of thin section samples was carried out at the Key Laboratory of Marine Geology, Tongji University. Before the preparation of thin sections, all samples were repeatedly washed with pure water to completely eliminate mud interference, followed by drying using a dryer. After drying, the samples were not stained and were prepared into microscopic thin sections following the rock thin section identification standard SY/T 5368–2016 [58], with a specification of 50  $\mu\text{m}$ . Observations of the thin sections were conducted using the Mshot MP41 professional polarizing microscope (Mshot, Guangzhou, China) [59,60]. The main observations included mineral composition, particle size, sorting, rounding, clastic types, and rock types.

##### 3.2.3. Core Observation

Before starting the core observations, the cores were wiped and cleaned with distilled water to avoid the impact of covering dust. After air drying, photographs of the cores were taken using a Huawei P40 device (Huawei, Shenzhen, China) equipped with a Leica triple camera (50 MP Ultra Vision Wide Angle Lens f/1.9 +, 16 MP Ultra-Wide Angle Movie Lens f/2.2 +, 8 MP Telephoto Lens f/2.4 OIS +, Leica, Wetzlar, Germany). The focus of the observations was on rock types, lithological combinations, particle sizes, clastic types, and roundness [61].

Through the observation of cores from the Cretaceous section and microscopic thin sections, combined with the basic lithological data of borehole A-1, a detailed description of the petrological characteristics and lithological combinations of segmented sections of bore-

hole A-1 was achieved. This allowed for a preliminary inference of the main sedimentary facies types in the western part of the Qiantang Depression during various periods.

### 3.2.4. Detrital Zircon Sample Preparation and Analysis Methods

By comparing the ages of detrital zircons to the age of strata in the source area, the provenance of sediments can be definitively ascertained [62,63]. Regrettably, not only Cretaceous strata but also all the sedimentary layers of different ages in Qiantang Sag have not undergone detrital zircon source analysis, leaving us without direct data from the area. Fortunately, this research obtained valuable drilling samples, allowing us to conduct the first detrital source analysis of the Qiantang Sag. This part of the study focused on the Cretaceous strata of the western Qiantang Sag, employing LA-ICP-MS detrital zircon U-Pb geochronology to define the depositional age of strata and to explore and reveal their source evolution characteristics.

To gain a deeper understanding of the sedimentary sources of the Qiantang Sag, systematic sampling was conducted on the sole drilling borehole, borehole A-1. The samples included detrital sandstone from the contact of the Upper Cretaceous and Paleocene, the lowermost of the Upper Cretaceous, and the lowermost of the Lower Cretaceous. The samples were crushed and sieved to 70 mesh (212  $\mu\text{m}$ ) at the State Key Laboratory of Marine Geology at Tongji University, then sent to Langfang Quanxin Geological Technical Service Co., Ltd. (Langfang, China) for washing, electromagnetic and heavy liquid separation. Afterwards, under a binocular microscope, zircons with complete crystal shapes and larger grain sizes were selected for subsequent analysis. The samples were then sent to Nanjing Zhuyan Space Technology Co., Ltd. (Hangzhou, China) for further processing, where zircons with complete crystal shapes and larger grains were targeted, and about 150 grains per sample were glued with colorless transparent epoxy resin. After the resin solidified, the zircons were polished, and high-definition cathodoluminescence images and transmitted and reflected light photographs of the zircon targets were taken. Based on the internal structure, inclusions, and grain size of the zircons, suitable locations for laser ablation were determined.

The LA-ICP-MS zircon U-Pb dating test was conducted at Nanjing Jupu Detection Technology Co., Ltd. (Nanjing, China) It utilized a 193 nm ArF excimer laser ablation system (Analyte Excite) manufactured by Teledyne Cetac Technologies (Omaha, NE, USA) and an Agilent 7700x quadrupole ICP-MS manufactured by Agilent Technologies (Santa Clara, CA, USA). The deep ultraviolet beam generated by the excimer laser was focused on the zircon surface through a homogenizing optical path, with an energy density of 6.0 J/cm<sup>2</sup>, a beam diameter of 35  $\mu\text{m}$ , a frequency of 8 Hz, and an ablation time of 40 s. The ablated aerosol was introduced into the ICP-MS with helium gas [64]. The standard zircon 91,500 [65] was used to correct instrument mass discrimination and elemental fractionation during the test process; standard zircon GJ-1 was used as a blind sample to verify the quality of U-Pb dating data; and NIST SRM 610 [66] was used as an external standard, with Si as an internal standard for calibrating Pb content in zircon, and other trace elements calibrated against Zr. The raw test data were processed offline using ICPMS DataCal software v4.6 [67,68]. The U-Pb age Concordia plots were created using Isoplot software 4.0 [67,68]

## 4. Results

### 4.1. Stratigraphic Characteristics and Sedimentary Sequence

#### 4.1.1. Sag Structure and Stratigraphic Distribution

The Qiantang Sag is a typical rift basin and hosts the thickest residual strata in the central part of the ECS Shelf Basin. These massive sedimentary strata are primarily Mesozoic, followed by the Paleogene's Paleocene and Eocene formations [6,35,36]. The Mesozoic and Cenozoic strata explicitly revealed by drilling reach a thickness of 3600 m. Seismic profile interpretation suggests the existence of Jurassic strata in the Qiantang Sag that were not encountered by drilling. It is estimated that the total thickness of sedimentary deposits in the central part of the Qiantang Sag could exceed 4000 m (Figures 2 and 3).

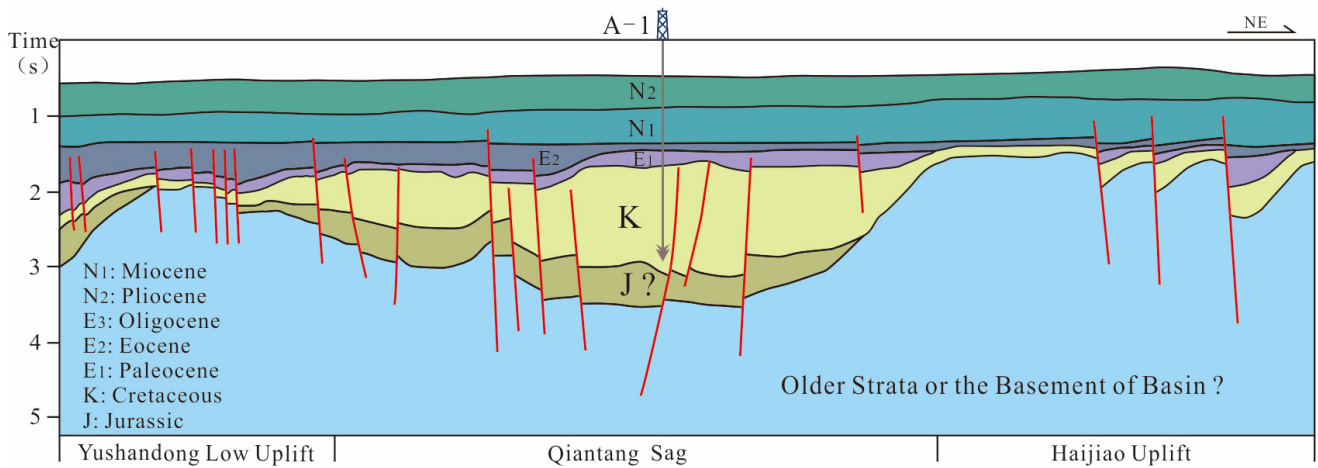


**Figure 2.** Line 1 seismic geological interpretation profile through the Yushan Dong Uplift–Qiantang Sag–Haijiao Uplift.

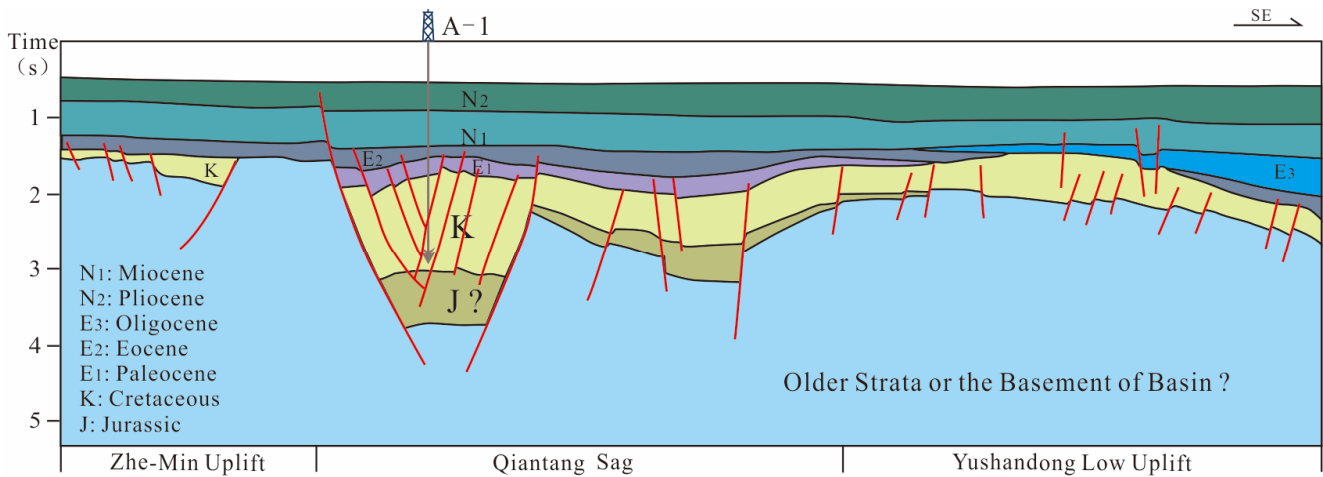


**Figure 3.** Seismic geological interpretation profile through the Zhe-Min Uplift–Qiantang Sag–Yushan Dong Uplift.

The sedimentary Mesozoic strata remaining in the Qiantang Sag are exceptionally thick. The Mesozoic Cretaceous strata encountered by drilling exceed 2000 m. Based on seismic geological interpretation profiles, the thickness of the Jurassic strata in the Qiantang Sag is mainly between 400 and 1900 m, with the maximum thickness located at the center of the sag. The thickness of the Cretaceous strata ranges from 400 to 3000 m, predominantly situated in the southern part of the Qiantang Sag. The seismic profiles of the Mesozoic strata in the Qiantang Sag primarily show weak vibrations, medium-poor continuity, and medium-low frequency, making it difficult to accurately identify the seismic facies. It is generally conjectured that these sedimentary layers are likely continental deposits.

#### 4.1.2. Vertical Stratigraphic Features and Sedimentary Sequence

Borehole A-1, the sole exploratory borehole in the Qiantang Sag, is located in the southwestern part of the sag and reaches a total depth of 4501 m. It encountered Mesozoic strata up to 2650 m thick, all belonging to the Cretaceous system. The Lower Cretaceous comprises 600 m of the Yushan Formation, and the Upper Cretaceous exceeds 2000 m, identifying two main strata: the Shimentan and Minjiang Formations (Figure 4).

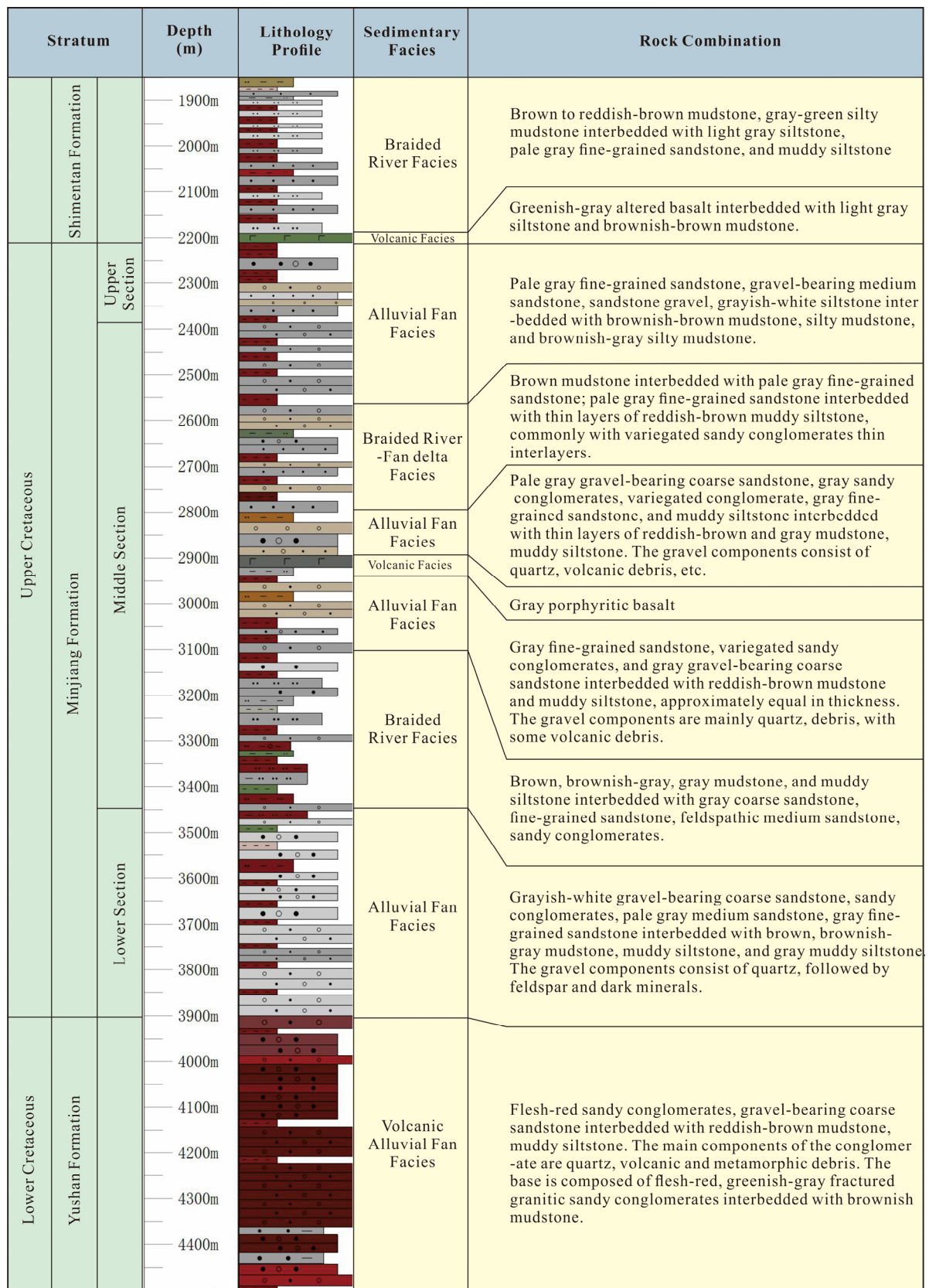
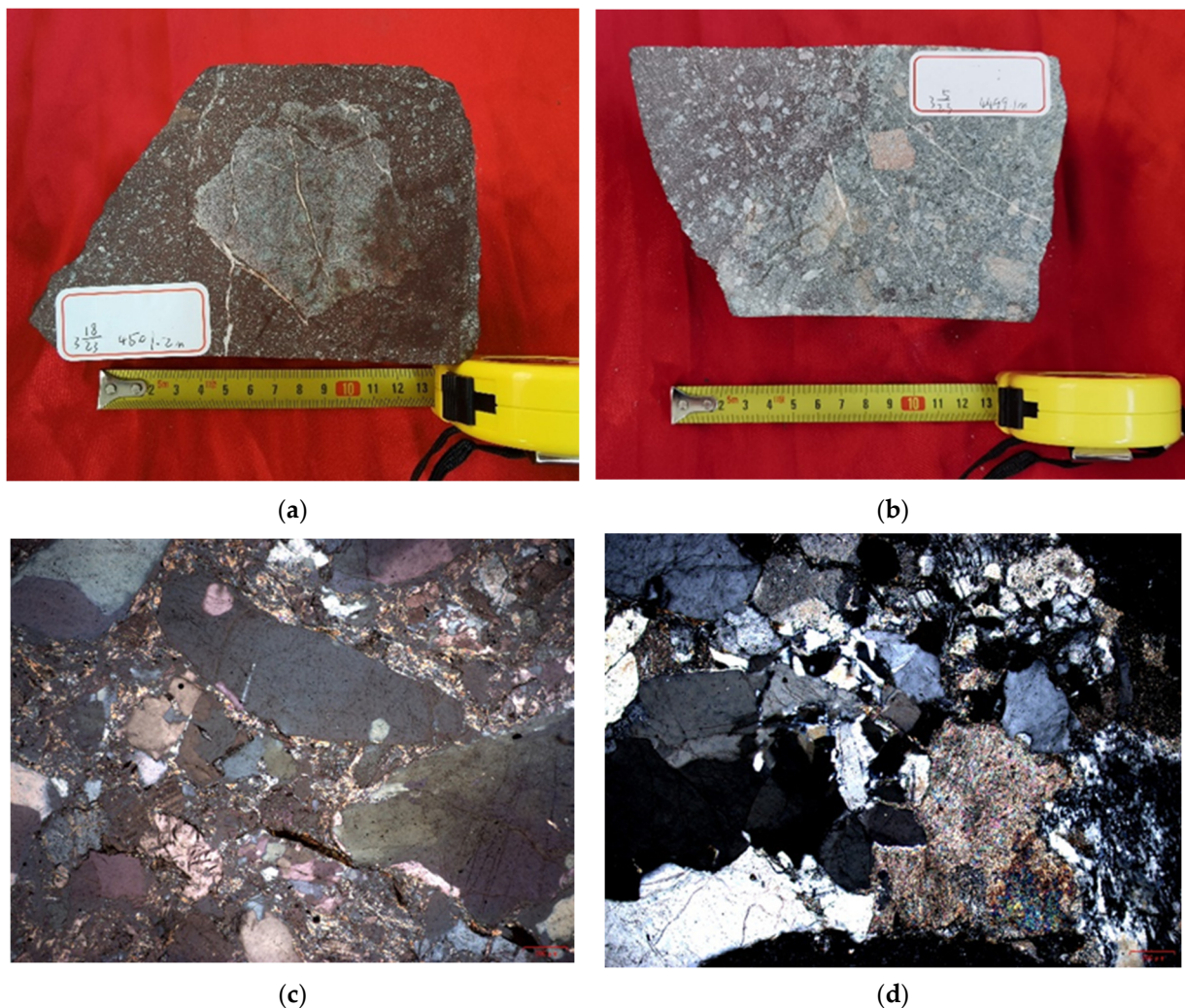


Figure 4. Composite sedimentary succession for the Cretaceous Strata in the Qiantang Sag.



The Lower Cretaceous Yushan Formation represents typical Cretaceous red beds, primarily composed of flesh-red and gray-green conglomerates, coarse-grained sandstones with gravel, and brownish-red mudstone and silty mudstone in continuous interbedding relationship (Figure 4). The conglomerates mainly consist of quartz, volcanic, and metamorphic rock fragments. Granules range from 2 to 4 mm, while larger clasts range in size from 1 to 4 cm, with some even reaching up to 8 cm. These are poorly sorted and exhibit angular to sub-angular shapes (Figure 5). At the base of the Yushan Formation, there is a layer of flesh-red and greenish-gray fractured granitic conglomerate interbedded with brownish mudstone, with large granitic fragments visible (Figure 5a,b). The mudstones locally contain rock fragment clasts and crystals of feldspar and quartz, and they are relatively hard. (Figure 5). Such characteristics show strong similarities to the continental rift valley red beds formed under oxidizing conditions in a continental environment, as found in southern New England, USA [69,70]. This lithological sequence suggests a typical arid alluvial fan deposit influenced by intense volcanic activity, and the grain size, sorting, and morphology of the clastic particles indicate likely proximal deposits.



**Figure 5.** Stratigraphic Features of the Lower Cretaceous Yushan Formation in the Qiantang Sag. (a) Giant greenish-gray fractured granitic clasts at 4501.2 m; (b) conglomerate mudstone with sandstone and gravel at 4499.1 m; (c) microscopic features of quartz clastic conglomerate sandstone at 4500.7 m; (d) microscopic features of feldspar clastic conglomerate sandstone at 4479 m.

The Upper Cretaceous Minjiang Formation, encountered in borehole A-1, represents the thickest secondary stratigraphic unit, reaching a depth of 1700 m. This considerable thickness allows for greater diversity in the vertical lithological composition (Figure 4). The lower section consists of interbedded layers of greyish-white coarse sandstone with gravel, conglomerates, light grey medium sandstone, grey fine sandstone, and brownish-grey to grey mudstone and siltstone. The gravel primarily comprises quartz, followed by feldspar and dark minerals. This composition indicates a period of reduced magmatic activity. However, despite the subdued magmatic activities, the sedimentation environment was still characterized as an alluvial fan under semi-arid conditions with episodic high-energy flow but insufficient duration of hydrodynamics to create rounding and sorting.

Progressing upwards, the formation shows layers of brown, greyish-brown, and grey mudstone; siltstone with grey coarse sandstone, fine sandstone, and feldspar-bearing medium sandstone; and conglomerates (Figure 6). The detrital components of the sandstone predominantly exhibit fewer magmatic rock fragments and demonstrate improved sorting, along with a slight enhancement in hydrodynamic conditions. The coloration of the mudstones points toward a likely oxidizing environment, which is indicative of deposits typically formed in braided river systems within a semi-arid alluvial fan setting.

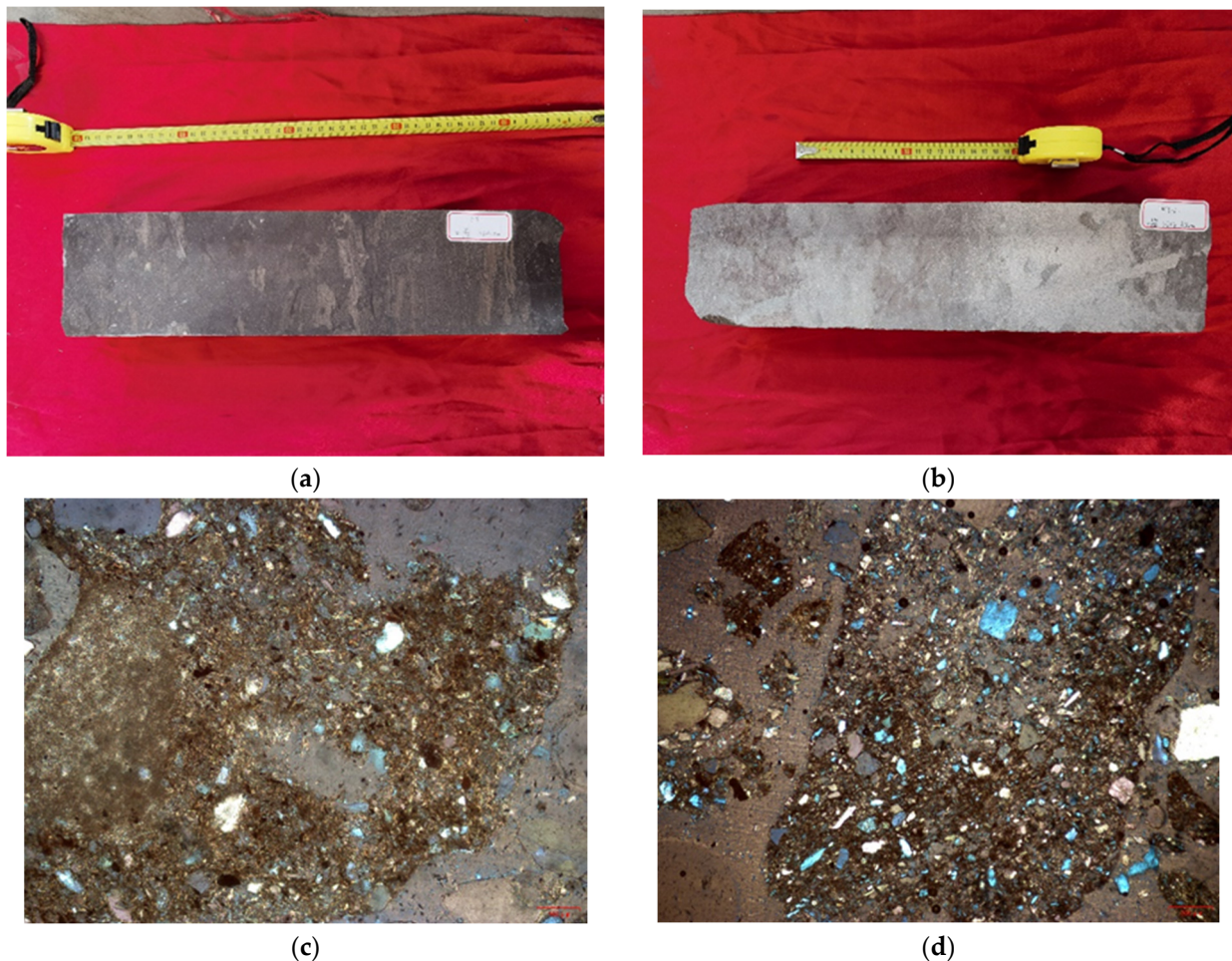


**Figure 6.** Features of the Upper Cretaceous Minjiang Formation in the Qiantang Sag. (a) Brown siltstone mudstone at 3316 m; (b) greyish-white gritty fine sandstone (gravelly fine sandstone) at 3314.8 m; (c) microscopic features of sandy mudstone at 3485 m; (d) microscopic features of siltstone mudstone at 3485 m.

Notably, in the middle section of the Minjiang Formation, grey tholeiitic basalt layers were identified (Figure 7), with increased magmatic rock fragments in the surrounding clastic deposits. These included medium to coarse sand-sized grains predominantly of quartz and lithic fragments, with conglomerates mainly composed of volcanic rock fragments, exhibiting colors like flesh-red, grey-white, and grey-black. The fragments, ranging from 3 to 5 mm in size, showed poor sorting and sub-angular shapes. Despite the thickness of the basalt layers and characteristics of the basaltic magma flow, it is inferred that no intense volcanic eruption occurred near the A-1 borehole. However, during this period, there might have been instances of basaltic magma extruding through fissures in the strata to the surface, consistent with the vertical characteristics of the aforementioned strata.

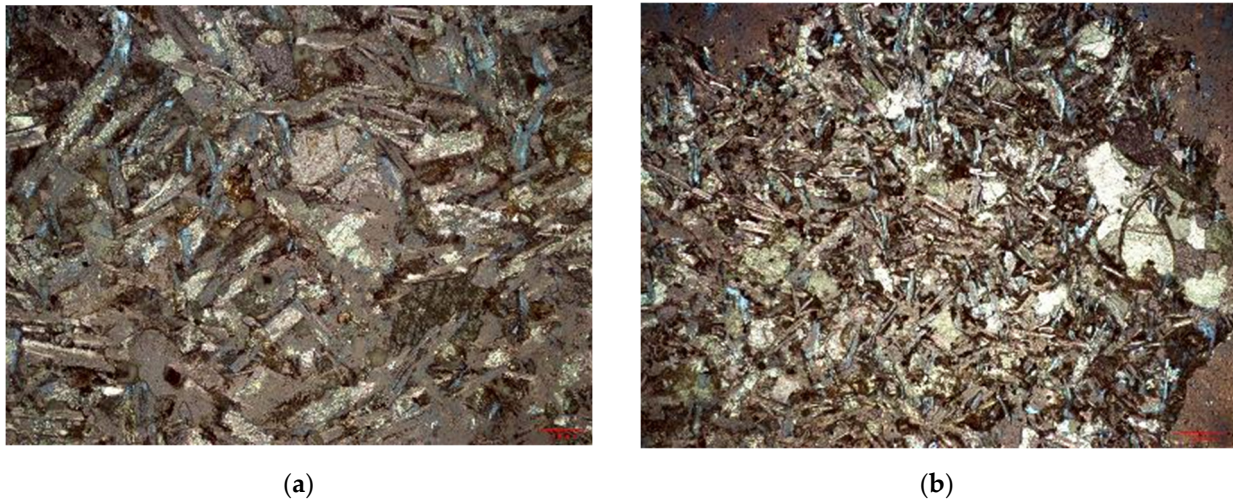


**Figure 7.** Microscopic features of basalt in the middle section of the Upper Cretaceous Minjiang Formation in the Qiantang Sag. (a,b) Tholeiitic basalt with blastoporphyritic texture.

The upper Cretaceous Shimentan Formation is relatively thin, with a thickness of about 300 m. At the base of the Shimentan Formation, a set of green-gray altered basalt, light gray silty sandstone, and brownish mudstone are interbedded (Figure 4). This stratigraphic sequence is in disconformable contact with the underlying layers, indicating another instance of basaltic magma overflowing along fissures, though on a smaller scale compared to the Minjiang period (Figure 4). The middle and upper parts of the Shimentan Formation comprise brown, reddish-brown mudstone; gray-green silty mudstone; gray-white silty sandstone; light gray fine sandstone; and silty sandstone mudstone interlayers (Figure 8). Considering the prevalent formation of red beds in South China and adjacent regions during the Cretaceous, primarily in arid to semi-arid sedimentary environments, the red coloration of the mudstones here suggests an oxidizing environment characteristic of these dry conditions. However, given the improved sorting observed in these rock sequences, it suggests that hydrodynamic conditions experienced an enhancement and relative stability, indicative of deposits typical of semi-arid alluvial fans and braided rivers. Moreover, the lithological variation locally displays deltaic traits, hinting at the existence of significant braided rivers and seasonal lakes at times, possibly including fan deltas or braided river deltas.



**Figure 8.** Core features of the Upper Cretaceous Shimentan Formation in the Qiantang Sag. (a,b) Brownish mudstone and silty siltstone at 2027 m.

#### 4.2. Detrital Zircon Provenance Analysis

The analysis results are as follows (Figure 9):

1. Samples from the contact position between the Upper Cretaceous and Paleocene formations (at a depth of 1832 m): A total of 70 zircon grains were tested, with grain sizes ranging from 50 to 150  $\mu\text{m}$ . Some zircon grains were darker in color, and some lacked oscillatory zoning, possibly indicating a metamorphic origin. The overall Th content ranged from 52.8 to 1302.2 ppm, U content from 58.1 to 1620 ppm, with Th/U ratios of 0.14–2.36. A portion of the ages were scattered, with 59 ages falling on or near the Concordia line, mainly concentrated in the range of 130–90 Ma.

2. Samples of clastic sandstone from the lowermost part of the Upper Cretaceous (at a depth of 3856 m): A total of 120 zircon grains were analyzed, with grain sizes ranging from 50 to 140  $\mu\text{m}$ . The zircons were colorless or slightly brownish, with developed oscillatory zoning. The overall Th content varied between 61.2 and 2084 ppm and U content between 76.9 and 1246.5 ppm, with Th/U values ranging from 0.12 to 1.77. The majority of the ages fell on or near the Concordia line, primarily concentrated around 105 Ma, with the main distribution being between 110 and 100 Ma.

3. Samples of clastic sandstone from the lowermost part of the Lower Cretaceous (at a depth of 4479 m): A total of 120 zircon grains were analyzed, with grain sizes ranging from 70 to 250  $\mu\text{m}$ . The zircons exhibited well-developed oscillatory zoning and intact crystal forms. The overall Th content ranged from 16 to 1851.1 ppm and U content from 53.3 to 1431.3 ppm, with Th/U values between 0.02 and 2.4. Most of the ages, barring a few scattered ones, fell on or near the Concordia line, predominantly concentrated around 106 Ma, with a primary distribution between 120 and 100 Ma.

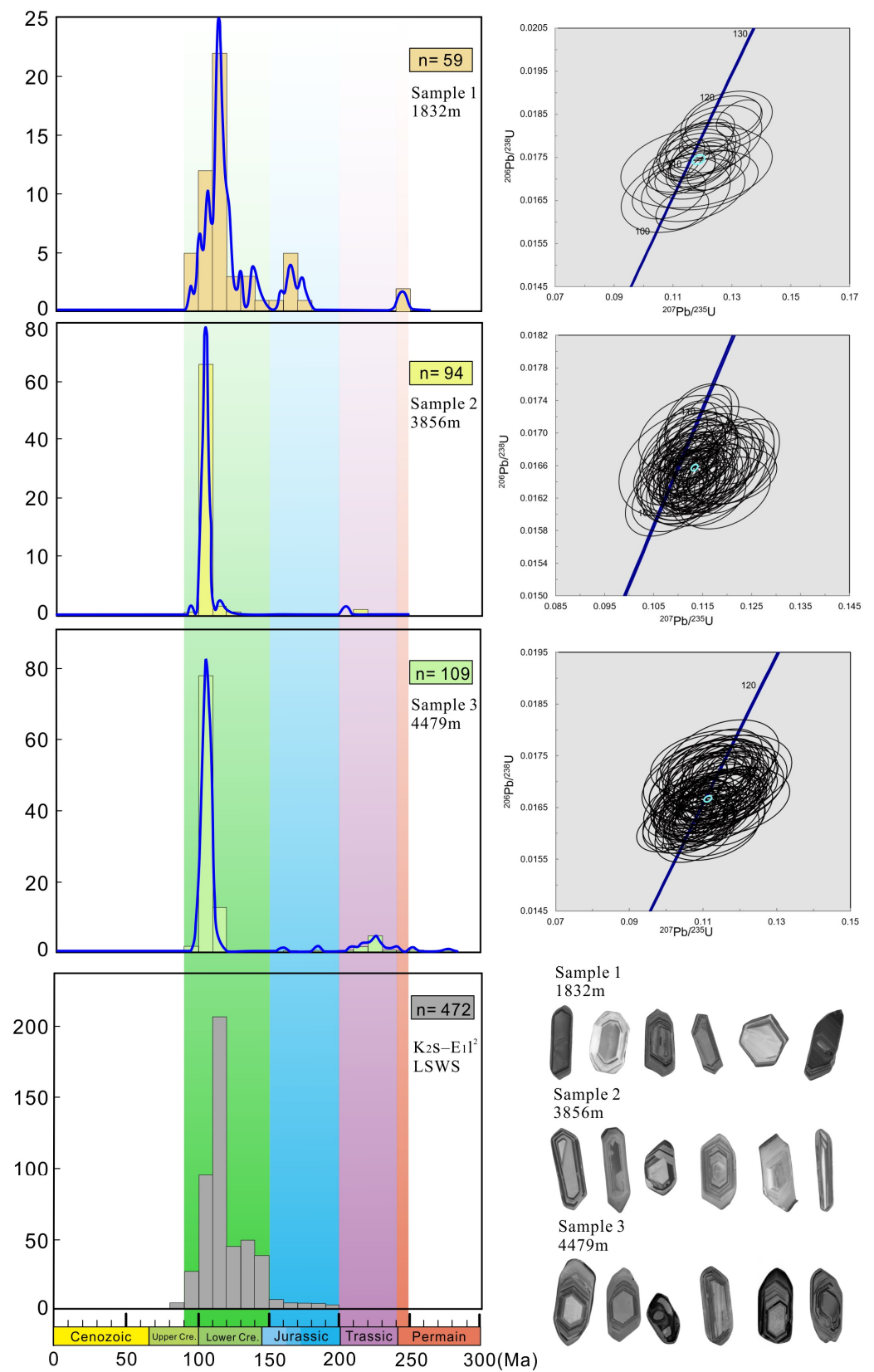


**Figure 9.** Comparison of detrital zircon age spectra between samples from the Cretaceous Strata of the Qiantang Sag and the West Lishui Subbasin (LSWS). The data for LSWS are derived from Reference [64].

## 5. Discussion

### 5.1. Discussion on Provenance

Sedimentary provenance analysis is fundamental to studying source-to-sink systems and is of prospective significance in sedimentology, reservoir geology, and petroleum geology [71]. In the Qiantang Sag, provenance analysis is crucial for discussing sedimentary evolution patterns. Given the limited number of drilling boreholes and the poor quality of seismic data in the area, scientifically reconstructing the sedimentary evolution model necessitates provenance analysis to identify the main source areas. This, combined with the sag's structure, stratigraphic distribution, and vertical sedimentary sequences, allows for the construction of a scientifically sound sedimentary evolution model.

Despite the long-term lack of substantial progress in sedimentary provenance analysis for the Qiantang Sag, based on the results of the aforementioned studies, a certain understanding of the sedimentary provenance during the Cretaceous period of the Qiantang Sag has been gained. Firstly, considering the structure and stratigraphic distribution of the sag (Figures 2 and 3), it is a typical rift basin, controlled by faults. Some scholars speculate that the Qiantang Sag was in the rift stage during the Mesozoic era [35,36,48]. Rift basins primarily develop proximal deposits during the rifting stage [72]. Based on the basin type to which the Qiantang Sag belonged during the Mesozoic era, it is inferred that the Qiantang Sag may have also developed proximal sedimentation during this period.

Secondly, the analysis of the vertical sedimentary sequence revealed that the Cretaceous strata of borehole A-1 predominantly consist of alluvial fan-braided river facies. This indicates that during the Cretaceous Period, especially in the early Cretaceous, the development of alluvial fan deposits was more pronounced in the western part of the Qiantang Sag, which is a typical feature of proximal deposition [73]. The sedimentary characteristics of the Cretaceous system in the Qiantang Sag thus highlight the aspect of proximal deposition.

From a regional perspective, the western part of the Qiantang Sag is adjacent to the Zhe-Min Uplift. During the Cretaceous Period, there was a significant elevation difference between these two areas, with a sudden change in slope gradient [6,48]. The uplift provided clastic material sources for multiple depressions in the vicinity. Other major uplifts in the surrounding areas are located at a certain distance from the Qiantang Sag. Therefore, it can be inferred that the western part of the Qiantang Sag predominantly developed proximal deposits, and the main source of these deposits was likely from the Zhe-Min Uplift to the west.

To precisely explore the provenance evolution in the western part of the Qiantang Sag, detrital zircon age analysis provides the most compelling evidence [74,75]. Zircons are extremely stable, maintaining stability and isotopic system closure in processes like weathering, transport, sedimentation, diagenesis, and even low-grade metamorphism. Detrital zircon dating is a crucial method for provenance analysis, as the ages revealed by this technique can reliably constrain the age of sedimentary layers, particularly those lacking fossil evidence.

Detrital zircon provenance analyses from three different beds in borehole A-1 exhibit a characteristic unimodal age spectrum, predominantly within the range of 90–110 Ma (Figure 9). This age distribution guides the investigation into the potential source areas' rock units and their ages, associated with the peripheral tectonic structures.

Within the western depression belt of the ECS Shelf Basin, the Lishui Sag in the south, like the Qiantang Sag, is proximal to the Zhe-Min Uplift to its west [76–78]. This location of the Lishui Sag offers an indirect basis for contrasting the provenance relations between the Qiantang Sag and the Zhe-Min Uplift.

Compared to the Qiantang Sag, the provenance study of the Lishui Sag is more comprehensive. Some researchers suggest that analyses of detrital zircon ages and rare earth element partitioning patterns indicate west Lishui Sub-sag (LSWS)'s provenance originates from the Zhe-Min Uplift, with no evident source variation among different strata [62]. Other

researchers have noted that in the upper strata of the Mingyuefeng Formation (E1m) in the Lishui Sag, the provenance from the Zhe-Min Uplift area is predominantly evident [77].

However, before the submergence of the Lingfeng barrier, the western subsags of the Lishui Sag were also dominated by proximal deposition, with the primary provenance being from the Zhe-Min Uplift to its west [78]. The Shimentan to Upper Lingfeng Formations (K<sub>2</sub>S–E<sub>1</sub><sup>L2</sup>) provide 472 age data points from the LSWS [78]. U-Pb age comparison of detrital zircons (with concordance  $\geq 90\%$ ) between the western Lishui Subsag (post-Lingfeng barrier submergence) and three samples from the Qiantang Sag reveals a high degree of similarity. This further demonstrates the highly similar age background of detrital provenance between the aforementioned source areas and the depositional basin.

Considering the aforementioned age characteristics of source–sink detrital provenances, in conjunction with the structural and stratigraphic distribution characteristics of the Qiantang Sag, the vertical depositional sequences revealed by drilling, and the inter-regional relationships, it becomes evident that the primary source area for the western part of the Qiantang Sag is the adjacent Zhe-Min Uplift. Although a small number of Jurassic and Triassic age detrital zircons are observed in the samples from the top part of the Upper Cretaceous, this might be attributed to the Late Cretaceous arc-ward sea jump [40], resulting in intense arc-back erosion and widespread erosional areas, leading to the Qiantang Sag potentially receiving minor provenance from more distant sources. Overall, it is still considered that the source supply from the Zhe-Min Uplift on the west is the primary contributor to the Cretaceous strata deposition in the western part of the Qiantang Sag.

## 5.2. Discussion on Sedimentary Models

### 5.2.1. Discussion of Key Conditions

In the Cretaceous vertical depositional sequence revealed by the A-1 borehole, features indicative of alluvial fan sedimentation such as significant grain size variability, poor sorting, and angularity were identified (Figures 4–8). These characteristics resonate with the Cretaceous provenance analysis results (Figure 9). Considering the characteristics of proximal deposition, it is inferred that during the Cretaceous Period, the Qiantang Sag was predominantly characterized by alluvial fan deposition.

The formation of alluvial fans necessitates multiple conditions [79]. Firstly, Within the tectonic context of the study area, orogenic activity may be one of several potential factors contributing to the formation of alluvial fans. The main provenance area of the western Qiantang Sag–Zhe-Min Uplift is a result of such orogenic movements. This orogenic activity enhanced erosion in the source area and river energy, leading to the transport of a large amount of detrital material, thus forming extensive alluvial fans.

Secondly, arid and semi-arid climatic conditions often provide a substantial supply of detrital material for the formation of alluvial fans, especially in the context of South China and adjacent areas, which are predominantly characterized by oxidative sedimentary environments developed under arid and semi-arid conditions. It is inferred that the brownish-red and reddish-brown hues of the Cretaceous mudstones observed in the A-1 borehole also reflect such sedimentary environments [80,81].

Furthermore, a sudden change in topographic gradient is also crucial for the formation of alluvial fans. Seismic geological interpretations reveal a significant elevation difference between the Zhe-Min Uplift and the Qiantang Sag. The abrupt change in terrain leads to a rapid reduction in mountainous river flow, resulting in extensive deposition of detrital materials at the foothills.

Lastly, for vertically superimposed fans, prolonged relative tectonic subsidence is necessary [72], and the Qiantang Sag, being a rift basin during the Mesozoic era, provided such subsidence conditions, favorable for the preservation of alluvial fans.

### 5.2.2. Multi-Phase Sedimentary Evolution Model

The study on the evolutionary pattern of Cretaceous sedimentation in the western Qiantang Sag is based on the tectonic and stratigraphic distribution characteristics of the Qiantang Sag. Combined with the vertical depositional sequence of the A-1 borehole, integrated with the primary provenance areas and directions and the characteristics of proximal deposition, this leads to the inference of a multi-phase sedimentary evolution model for the western Qiantang Sag during the Cretaceous Period.

During the Yushan period of the Early Cretaceous, influenced by the accelerated subduction of the ancient Pacific Plate, the Zhe-Min Uplift experienced intense volcanic activity. The severe volcanic activity and magmatic intrusion introduced a substantial amount of magmatic rock detritus to the uplift area. Accompanied by rapid changes in river energy, large alluvial fans developed in the adjacent western Qiantang Sag (Figure 10). At this time, the hydrodynamic force was episodic, characterized mainly by the presence of abundant volcanic detritus in an arid environment and the uneven distribution of water flow in alluvial fan deposits.

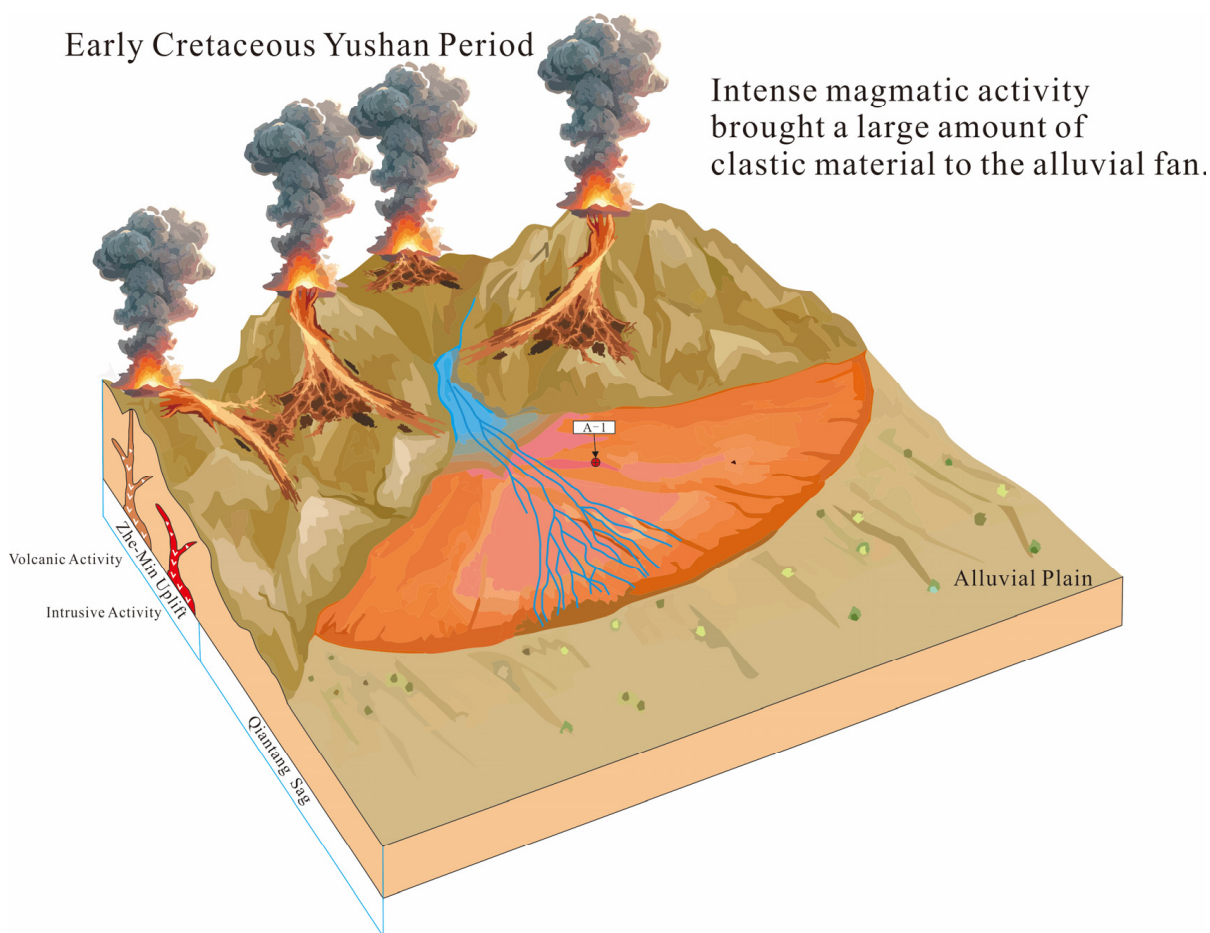


**Figure 10.** Sedimentary model diagram of the Early Cretaceous Yushan period in the western part of the Qiantang Sag.

During the Minjiang period of the Late Cretaceous, volcanic activity relatively diminished, leading to a reduced impact of volcanic activity in the western region of the Qiantang Sag. Despite this, the main supply of detrital material still originated from the Zhe-Min Uplift to the west. As the uplift area receded and hydrodynamic force increased, the original alluvial fans gradually retreated, and the influence of fluvial deposition correspondingly expanded. Given the climatic characteristics of the broader regional area at that time, it is inferred that the area remained in an oxidizing environment, exhibiting interbedded



depositional characteristics of alluvial fans and braided rivers, driven by periodic changes in hydrodynamics (Figure 11). Although volcanic activity in the Zhe-Min Uplift weakened, magmatic activity in the Qiantang Sag persisted. In the mid-Minjiang Period, magma overflowed along faults, covering parts of the western Qiantang Sag. As this magmatic event was short-lived and did not form thick basaltic deposits, it still provided a certain amount of detrital material for the mid-Minjiang Period alluvial fan-braided river deposits.

### Late Cretaceous Minjiang Period

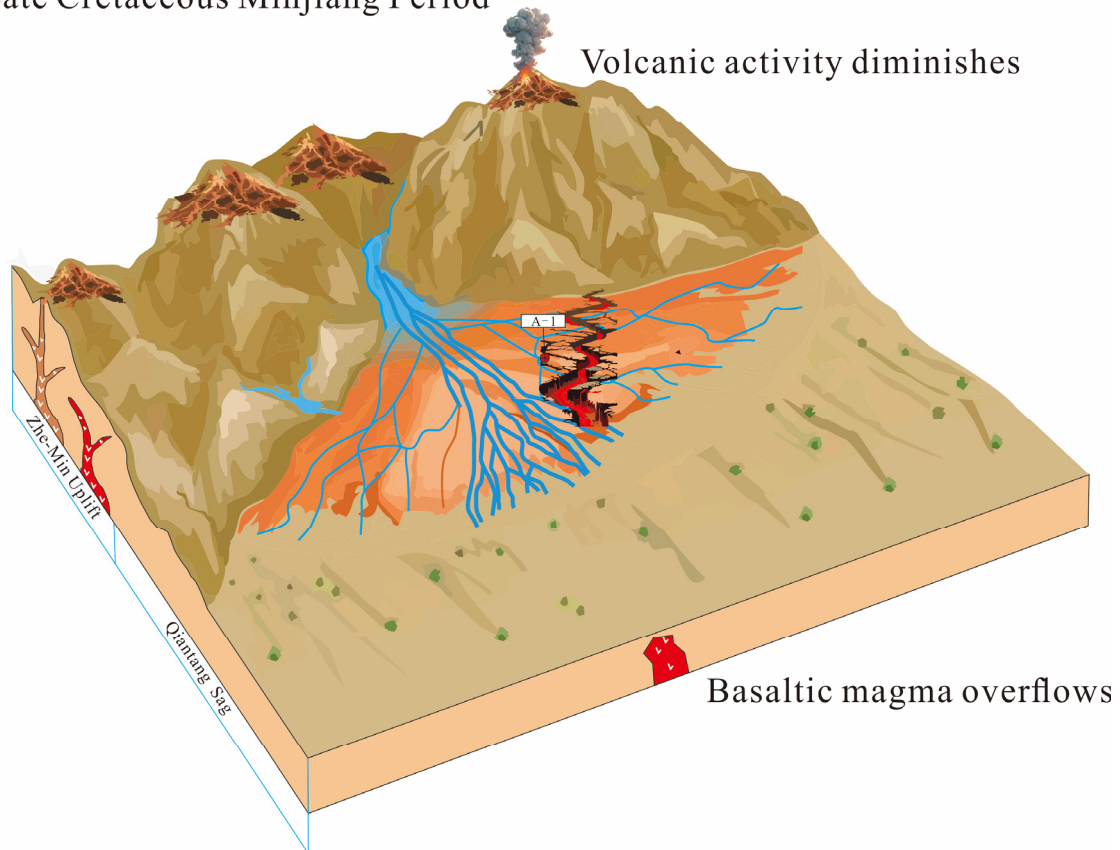


**Figure 11.** Sedimentary model diagram of the Late Cretaceous Minjiang period in the western part of the Qiantang Sag.

During the Shimentan period of the Late Cretaceous, magmatic activity within the region further subsided. With the decline of volcanic activity in the Zhe-Min Uplift to the west, there was only a brief episode of basaltic magma overflow along faults during the early part of this period. This suggests that external forces began to dominate the sedimentation in the western part of the Qiantang Sag during the Shimentan Period (Figure 12). The continual influence of external forces led to further retreat of the uplift area, resulting in a corresponding reduction and shrinkage in alluvial fan deposits. The detrital materials provided by the Zhe-Min Uplift were transported to the western part of the Qiantang Sag by stronger hydrodynamic forces, leading to further expansion of the fluvial depositional area. In some cases, the hydrodynamic conditions here could be influenced by seasonal precipitation. During periods with stronger hydrodynamics, lakes might develop, as well as fan deltas or braided river deltas. However, the observation of mudstone colors indicates that the climate during this period still favored a semi-arid environment, suggesting that these lakes and deltas could be seasonal or intermittent phenomena.

## Late Cretaceous Shimentan Period

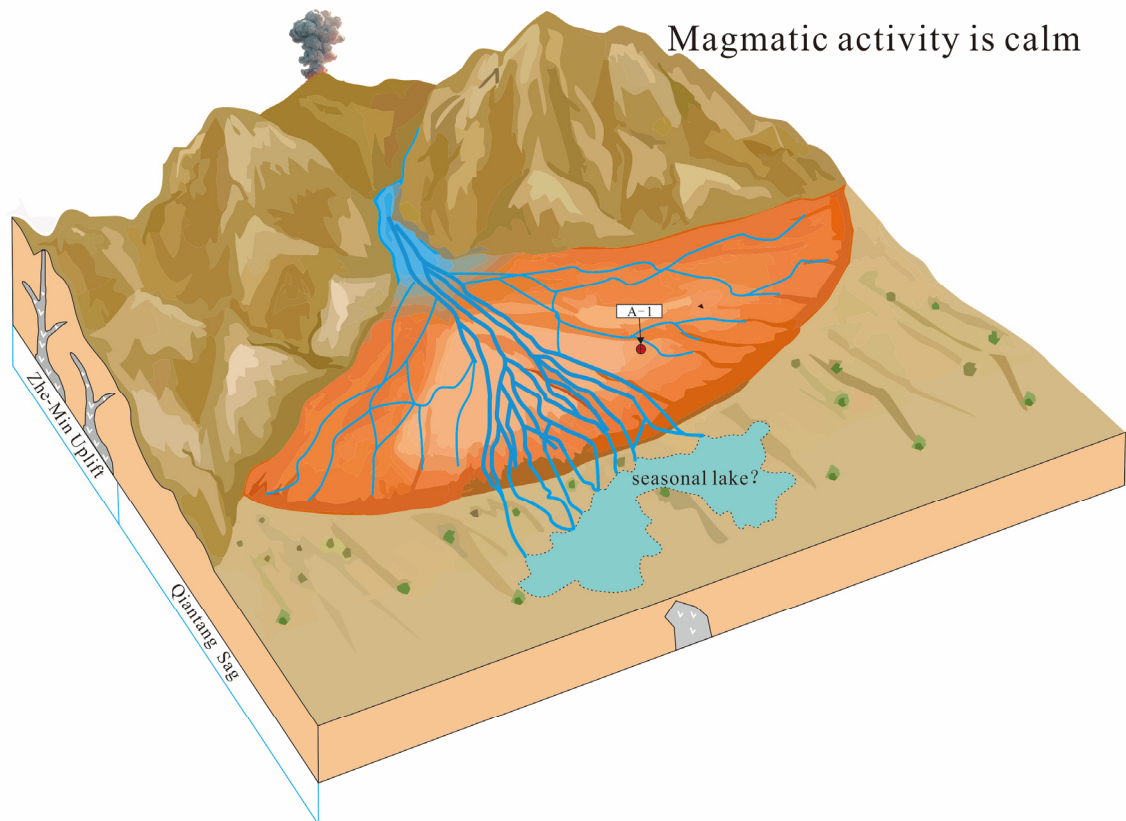


**Figure 12.** Sedimentary model diagram of the Late Cretaceous Shimentan period in the western part of the Qiantang Sag.

### 6. Conclusions

Based on the identification of the sag structure and stratigraphy, it has been discerned that the Qiantang Sag developed thick Cretaceous sedimentary strata. Furthermore, vertical sedimentary sequences have revealed the predominant development of alluvial fan-braided river deposits in arid to semi-arid environments in the western part of the Qiantang Sag during the Cretaceous.

Detrital zircon dating analysis of the Cretaceous samples from borehole A-1 reveals a typical unimodal age spectrum, predominantly concentrated around 90–110 Ma. Integrating the sag's structure and sedimentary characteristics, and by comparing with the provenance characteristics of the Lishui Sag, it is inferred that the western part of the Qiantang Sag developed proximal deposition, mainly sourced from the Zhe-Min Uplift to the west.

Synthesizing the aforementioned research evidence, it is posited that during the Early Cretaceous Yushan period, the western Qiantang Sag experienced arid alluvial fan deposition influenced by intense volcanic activity. During the Late Cretaceous Minjiang period, it underwent semi-arid alluvial fan-braided river deposition influenced intermittently by magmatic activity. In the Late Cretaceous Shimentan period, the region was characterized by semi-arid alluvial fan-braided river-seasonal lake deposits, influenced briefly by magmatic activity.

**Author Contributions:** Conceptualization, W.Z. and X.F.; methodology, X.F.; investigation, K.F., X.F., Z.Z., and L.H.; resources, X.F.; data curation, X.F.; writing—original draft preparation, K.F.; writing—review and editing, S.Z., W.C., and Z.Z.; visualization, K.F.; supervision, W.Z. and K.Z.; project administration, K.Z.; funding acquisition, W.Z. All authors have read and agreed to the published version of the manuscript.

**Funding:** This research was supported by the Open Fund (DGERA20231110) of the Key Laboratory of Deep-time Geography and Environment Reconstruction and Applications of Ministry of Natural Resources, Chengdu University of Technology.

**Institutional Review Board Statement:** Not applicable.

**Informed Consent Statement:** Not applicable.

**Data Availability Statement:** All data are contained within this article.

**Acknowledgments:** We express our sincere appreciation to the State Key Laboratory of Marine Geology at Tongji University for providing the necessary facilities and space for sample processing. We are profoundly grateful to Jingchun Tian from CDUT and Qiang Fu from TJU for their generous guidance and invaluable insights throughout our research. Our thanks also go to CNOOC and SINOPEC for their partial support with materials that significantly contributed to our study. Additionally, we would like to acknowledge the substantial assistance provided by Jinniu Chen and Qiang Hao from TJU during the revision process of our manuscript. Their contributions have been invaluable to the successful completion of our work.

**Conflicts of Interest:** The authors declare no conflicts of interest.

## References

- Hilde, T.W.C.; Uyeda, S.; Kroenke, L. Evolution of the western Pacific and its margin. *Tectonophysics* **1977**, *38*, 155–165. [[CrossRef](#)]
- Zhu, W.L.; Zhong, K.; Fu, X.W.; Chen, C.F.; Zhang, M.Q.; Gao, S.L. The formation and evolution of the East China Sea Shelf Basin: A new view. *Earth-Sci. Rev.* **2019**, *190*, 89–111. [[CrossRef](#)]
- Yang, C.; Li, S.Z.; Li, G.; Yang, C.; Yang, Y.Q.; Dai, L.; Suo, Y.; Li, Q.; Jiang, Y. Tectonic units and proto-basin of the East China Sea Shelf Basin: Correlation to Mesozoic subduction of the Palaeo-Pacific Plate. *Geol. J.* **2016**, *51*, 149–161. [[CrossRef](#)]
- Yang, C.; Sun, J.; Yang, Y.Q.; Yang, C.; Wang, J.; Xiao, G.; Wang, J. Key factors controlling Mesozoic hydrocarbon accumulation in the Southern East China Sea Basin. *Mar. Pet. Geol.* **2020**, *118*, 104436. [[CrossRef](#)]
- Su, A.; Chen, H.; Chen, X.; He, C.; Liu, H.; Li, Q.; Wang, C. The characteristics of low permeability reservoirs, gas origin, generation, and charge in the central and western Xihu Depression, East China Sea Basin. *J. Nat. Gas Sci. Eng.* **2018**, *53*, 94–109. [[CrossRef](#)]
- Zhong, K.; Wang, X.; Zhang, T.; Zhang, M.; Fu, X.; Guo, M. Distribution of residual Mesozoic basins and their exploration potential in the western depression zone of East China Sea Shelf Basin. *Mar. Geol. Quat. Geol.* **2019**, *39*, 41–51. (In Chinese with English Abstract)
- Zhong, K.; Zhu, W.; Gao, S.; Fu, X. Key geological questions of the formation and evolution and hydrocarbon accumulation of the East China Sea Shelf Basin. *Earth Sci.* **2018**, *43*, 3485–3497. (In Chinese with English Abstract)
- Li, S.; Shao, L.; Liu, J.; Qin, L.; Kang, S.; Eriksson, K.A. Oil generation model of the liptinite-rich coals: Palaeogene in the Xihu Sag, East China Sea Shelf Basin. *J. Petrol. Sci. Eng.* **2022**, *209*, 109844. [[CrossRef](#)]
- Ding, F.; Xie, C.; Zhou, X.; Jiang, C.; Li, K.; Wan, L.; Zhang, P.; Niu, H. Defining stratigraphic oil and gas plays by modifying structural plays: A case study from the Xihu Sag, east China Sea Shelf Basin. *Energy Geosci.* **2021**, *2*, 41–51. [[CrossRef](#)]
- Su, A.; Chen, H.; Cao, L.; Lei, M.; Wang, C.; Liu, Y.; Li, P. Genesis, source, and charging of oil and gas in Lishui sag, East China Sea Basin. *Pet. Explor. Dev.* **2014**, *41*, 574–584. [[CrossRef](#)]
- Ye, J.R.; Gu, H.R.; Jia, J.Y. Research on the hydrocarbon accumulation dynamics of Xihu Sag, East China Sea Shelf Basin. *J. Nat. Gas Ind.* **2005**, *25*, 5–8.
- Ye, J.R.; Qing, H.R.; Bend, S.L.; Gu, H.R. Petroleum systems in the offshore Xihu Basin on the continental shelf of the East China Sea. *AAPG Bull.* **2007**, *91*, 1167–1188. [[CrossRef](#)]
- Wang, D.; Li, H.; Lu, Y. Geochemical characteristics and distribution of Mesozoic hydrocarbon source rocks in the southern part of East China Sea. *Offshore Oil* **2015**, *35*, 1–6. (In Chinese with English Abstract)
- Zhu, X.; Chen, J.; Li, W.; Pei, L.; Liu, K.; Chen, X.; Zhang, T. Hydrocarbon generation potential of Paleogene coal and organic-rich mudstones in Xihu Sag, East China Sea Shelf Basin, offshore eastern China. *J. Pet. Sci. Eng.* **2019**, *184*, 106450. [[CrossRef](#)]
- Ruobing, L. Analysis of Hydrocarbon Exploration Potential in the Mesozoic of the Southern East China Sea Shelf Basin. *Offshore Oil* **2017**, *37*, 16–22. (In Chinese with English Abstract)
- Yang, C.; Yang, C.; Li, G.; Yang, Y.; Sun, J.; Yan, Z.; Wang, J. Prospecting of Meso-Cenozoic hydrocarbon in the East China Sea Shelf Basin. *Mar. Geol. Quat. Geol.* **2018**, *38*, 136–147. (In Chinese with English Abstract)
- Jiang, S.; Li, S.; Chen, X.; Zhang, H.; Wang, G. Simulation of oil–gas migration and accumulation in the East China Sea Continental Shelf Basin: A case study from the Xihu Depression. *Geol. J.* **2016**, *51*, 229–243. [[CrossRef](#)]
- Lee, G.H.; Kim, B.Y.; Shin, K.S.; Sunwoo, D. Geological evolution and aspects of the petroleum geology of the northern East China Sea shelf basin. *AAPG Bull.* **2006**, *90*, 237–260. [[CrossRef](#)]
- He, J.; Zhang, W.; Yan, W.; Lu, Z.; Zhang, J.; Gong, X. Episodic tectonic evolution, Basin types, and hydrocarbon accumulation in Chinese Marginal Basins. *Mar. Geol. Quat. Geol.* **2014**, *34*, 121–134. (In Chinese with English Abstract) [[CrossRef](#)]

20. Li, S.; Zhao, G.; Dai, L.; Liu, X.; Zhou, L.; Santosh, M.; Suo, Y. Mesozoic basins in eastern China and their bearing on the deconstruction of the North China Craton. *J. Asian Earth Sci.* **2012**, *47*, 64–79. [[CrossRef](#)]
21. Gong, J.; Li, G.; Yang, C.; Xu, X.; Zhang, J.; Wang, H.; Xu, L. Hydrocarbon Prospecting of Mesozoic Strata in Southern East China Sea Shelf Basin. *J. Jilin Univ.* **2013**, *43*, 20–27. (In Chinese with English Abstract)
22. Cukur, D.; Horozal, S.; Lee, G.; Kim, D.-C.; Han, H.-C. Timing of trap formation and petroleum generation in the northern East China Sea Shelf Basin. *Mar. Petrol. Geol.* **2012**, *36*, 154–163. [[CrossRef](#)]
23. Liang, X.; Chen, S.; Ma, B.; Ding, B.; Liang, Y.; Song, X.; Zhou, J.; Yu, Y.; Yu, L. Changes of tectonic regime of the East China Sea Shelf Basin since Mesozoic: Insights from the Tiantai slope belt, East China Sea. *J. Asian Earth Sci.* **2024**, *259*, 105900. [[CrossRef](#)]
24. Chen, J.; Li, G.; Chen, G. Petroleum prospects of Mesozoic and Paleocene in the western depression of the East China Sea shelf basin. *Mar. Geol. Lett.* **2003**, *19*, 17–19. (In Chinese with English Abstract)
25. Liang, J.; Chen, J.; Zhang, Y.; Yang, Y.; Li, G.; Li, Q.; Dong, G.; Yang, C. Type and origin of Mesozoic reservoirs in western depression zone of East China Sea shelf basin. *Mar. Geol. Quat. Geol.* **2016**, *36*, 131–138. (In Chinese with English Abstract)
26. Gurnis, M.; Turner, M.; Zahirovic, S.; DiCaprio, L.; Spasojevic, S.; Müller, R.; Boyden, J.; Seton, M.; Manea, V.C.; Bower, D. Plate tectonic reconstructions with continuously closing plates. *Comput. Geosci.* **2012**, *38*, 35–42. [[CrossRef](#)]
27. Hall, R. Cenozoic geological and plate tectonic evolution of SE Asia and the SW Pacific: Computer-based reconstructions, model and animations. *J. Asian Earth Sci.* **2002**, *20*, 353–431. [[CrossRef](#)]
28. Northrup, C.J.; Royden, L.H.; Burchfiel, B.C. Motion of the Pacific plate relative to Eurasia and its potential relation to Cenozoic extension along the eastern margin of Eurasia. *Geology* **1995**, *23*, 719–722. [[CrossRef](#)]
29. Changqing, Y.; Yanqiu, Y.; Gang, L.I.; Chuansheng, Y.; Jinyu, Y. The Mesozoic Basin-Mountain Coupling Process of the Southern East China Sea Shelf Basin and its Adjacent Land Area. *Acta Geol. Sin. (Engl. Ed.)* **2016**, *90*, 1051–1052. [[CrossRef](#)]
30. Han, H.-C.; Lee, Y.S.; Hwang, J.S.; Lee, S.-G.; Yoon, Y.; Stagpoole, V. Geophysical characteristics of the Hupijiao Rise and their implication to Miocene volcanism in the northeastern part of the East China Sea. *Mar. Geol.* **2015**, *363*, 134–145. [[CrossRef](#)]
31. Li, Z.X.; Li, X.H.; Chung, S.L.; Lo, Q.H.; Xu, X.S.; Li, W.X. Magmatic switch-on and switch-off along the South China continental margin since the Permian: Transition from an Andean-type to a Western Pacific-type plate boundary. *Tectonophysics* **2012**, *532*–535, 271–290. [[CrossRef](#)]
32. Xu, Q.-J.; Liu, S.; Wang, Z.; Zhang, B. Provenance of the East Guangdong Basin and Yong’an Basin in Southeast China: Response to the Mesozoic Tectonic Regime Transformation. *J. Asian Earth Sci.* **2019**, *185*, 104024. [[CrossRef](#)]
33. Lee, C.; Shinn, Y.J.; Ryu, I.C. Development of regional uplift and uplift-related strata in Gunsan Basin, Yellow Sea: Implications for Cenozoic crustal extension. *Int. Geol. Rev.* **2016**, *58*, 2029–2045. [[CrossRef](#)]
34. De-Zhang, G.; Jian, T.; Yu-Ling, B.O. Study on the Distribution of Mesozoic and Paleozoic Layer in Haijiao Doming and Qiantang Depression in the East China Sea. *Offshore Oil* **2005**, *25*, 1–6. (In Chinese with English Abstract)
35. Zhao, L. Study on Paleogene Sedimentary System of East China Sea Shelf Basin. Master’s Thesis, China University of Geosciences, Beijing, China, 2005. (In Chinese with English Abstract)
36. Xia, Q. Cenozoic Sedimentary System and Lithofacies Paleo-Geography in the East China Sea Shelf Basin. Master’s Thesis, China University of Geosciences, Beijing, China, 2005. (In Chinese with English Abstract)
37. Jiang, Y.; He, X.; Zhang, S. The Characteristics of “Inverse-transform” Tectonic Migration Evolution of the East China Sea Shelf Basin—By Taking the Marginal Structure of Xihu Sag for Example. *J. Yangtze Univ. (Nat. Sci. Ed.)* **2016**, *13*, 1–8. (In Chinese with English Abstract)
38. Guan, D.; Ke, X.; Wang, Y. Basement structures of East and South China Seas and adjacent regions from gravity inversion. *J. Asian Earth Sci.* **2016**, *117*, 242–255. [[CrossRef](#)]
39. Wang, Q.; Li, S.-Z.; Guo, L.-L.; Suo, Y.; Dai, L. Analogue modelling and mechanism of tectonic inversion of the Xihu Sag, East China Sea Shelf Basin. *J. Asian Earth Sci.* **2017**, *139*, 129–141. [[CrossRef](#)]
40. Zhu, W.; Xu, X.; Wang, B.; Cao, Q.; Chen, C.; Gao, S.; Feng, K.; Fu, X. Late Mesozoic continental arc migration in southern China and its effects on the evolution of offshore forearc basins. *Earth Sci. Front.* **2022**, *29*, 277–290. (In Chinese with English Abstract) [[CrossRef](#)]
41. Ding, W.; Li, J.; Wu, Z.; Li, S.; Lin, X. Late Mesozoic transition from Andean-type to Western Pacific-type of the East China continental margin—Is the East China Sea basement an allochthonous terrain? *Geol. J.* **2017**, *53*, 1994–2002. [[CrossRef](#)]
42. Suo, Y.; Li, S.-Z.; Zhao, S.-J.; Somerville, I.; Yu, S.; Dai, L.; Xu, L.; Cao, X.; Wang, P. Continental margin basins in East Asia: Tectonic implications of the Meso-Cenozoic East China Sea pull-apart basins. *Geol. J.* **2015**, *50*, 139–156. [[CrossRef](#)]
43. Wang, K.-L.; Chung, S.-L.; Lo, Y.; Lo, C.; Yang, H.; Shinjo, R.; Lee, T.; Wu, J.-C.; Huang, S. Age and geochemical characteristics of Paleogene basalts drilled from western Taiwan: Records of initial rifting at the southeastern Eurasian continental margin. *Lithos* **2012**, *155*, 426–441. [[CrossRef](#)]
44. Xu, C.; Zhang, L.; Shi, H.; Brix, M.; Huhma, H.; Chen, L.-H.; Zhang, M.; Zhou, Z. Tracing an early Jurassic magmatic arc from South to East China Seas. *Tectonics* **2017**, *36*, 466–492. [[CrossRef](#)]
45. Lin, A.T.; Watts, A.B.; Hesselbo, S.P. Cenozoic stratigraphy and subsidence history of the South China Sea margin in the Taiwan region. *Basin Res.* **2003**, *15*, 453–478. [[CrossRef](#)]
46. Xu, J.; Kelty, T.; Ben-Avraham, Z.; Yu, H. Origin of marginal basins of the NW Pacific and their plate tectonic reconstructions. *Earth-Sci. Rev.* **2014**, *130*, 154–196. [[CrossRef](#)]

47. Fu, X.; Ding, W.; Dadd, K.; Li, J.; Zhu, W.; Feng, K.; Geng, J.; Xu, X. An exotic origin of the eastern East China Sea basement before –150 Ma. *Sci. Bull.* **2022**, *67*, 1939–1942. [[CrossRef](#)] [[PubMed](#)]
48. Zhao, Y. Analysis of Oil and Gas Conditions of the Mesozoic in the East China Sea Shelf Basin. Master's Thesis, China University of Geosciences (Beijing), Beijing, China, 2005. (In Chinese with English Abstract)
49. Xu, C.; Deng, Y.; Barnes, C.G.; Shi, H.; Pascal, C.; Li, Y.; Gao, S.; Jiang, D.; Xie, J.; Ma, C. Offshore-onshore tectonomagmatic correlations: Towards a Late Mesozoic non-Andean-type Cathaysian continental margin. *Earth-Sci. Rev.* **2023**, *240*, 104382. [[CrossRef](#)]
50. Qiu, J.T.; Mu, H.X.; Rui, X.M.; Yang, Y.J.; Li, P.; Qiu, L.; Xu, C.B. The Relationships between Danxia Geoheritages and Regional Tectonics in Southern Sichuan Basin: Implications for the Spatial Distribution of Danxia Landforms in China. *Geoheritage* **2024**, *16*, 24. [[CrossRef](#)]
51. Liu, D.; Wang, C.; Zhang, X.; Hu, Y.; Wang, J.; Yan, K.; Yu, X.; Hu, H.; Lv, D.; Liu, X. Evidence of huge evaporite mine clusters under extreme arid climatic conditions of Cretaceous to Paleogene in South China: Example of the Huichang large salt deposit. *Ore Geol. Rev.* **2024**, *165*, 105899. [[CrossRef](#)]
52. Zheng, C.; Wang, J.; Li, X.; Zhang, C. Intermontane erg environment and arid climate indicated from associated eolian and alluvial fan facies during the Late Cretaceous, South China. *J. Asian Earth Sci.* **2024**, *264*, 106044. [[CrossRef](#)]
53. Chen, J.N.; Mao, X.G.; Shi, Y.H.; Liu, X.M. Study on the Late Cretaceous paleoenvironment documented by red beds in the western Fujian province. *Chin. J. Geophys.* **2020**, *63*, 1553–1568. [[CrossRef](#)]
54. Li, X.; Chen, S.; Cao, K.; Chen, Y.; Xu, B.; Ji, Y. Paleosols of the Mid-Cretaceous: A Report from Zhejiang and Fujian, SE China. *Earth Sci. Front.* **2009**, *16*, 63–70. [[CrossRef](#)]
55. Chen, L.; Guo, F.; Steel, R.; Li, Y. Petrography and geochemistry of the Late Cretaceous redbeds in the Gan-Hang Belt, southeast China: Implications for provenance, source weathering, and tectonic setting. *Int. Geol. Rev.* **2016**, *58*, 1196–1214. [[CrossRef](#)]
56. Yang, Y.; Jiang, Z.; Jiang, X. The Cretaceous Sedimentary Environments and Tectonic Setting of the Southern East China Sea Shelf Basin. *Energies* **2023**, *16*, 4205. [[CrossRef](#)]
57. Al-Masgari, A.A.; Elsaadany, M.; Latiff, A.H.A.; Imran, Q.S. A guideline for seismic sequence stratigraphy interpretation. *J. Eng. Appl. Sci.* **2021**, *16*, 165–183.
58. SY/T 5368–2016; Identification of Rock Flakes. The Standardization Administration of the People's Republic of China: Beijing, China, 2016.
59. Lai, J.; Wang, G.; Pang, X.; Fan, X.; Zhou, Z.; Si, Z.; Xie, W.; Qin, Z. Effect of Pore Structure on Reservoir Quality and Oiliness in Paleogene Dongying Formation Sandstones in Nanpu Sag, Bohai Bay Basin, Eastern China. *Energy Fuels* **2018**, *32*, 9220–9232. [[CrossRef](#)]
60. Zhao, S.; Fu, Q.; Fu, J.; Liu, X.; Li, S.; Zhang, G.; Teng, J. Effect of authigenic clay minerals and carbonate cements on quality of tight sandstone reservoirs: Insight from Triassic tight sandstones in the Huaqing area, Ordos Basin, Northern China. *J. Asian Earth Sci.* **2022**, *229*, 105099. [[CrossRef](#)]
61. Tian, J.; Liang, Q.; Wang, F.; Li, J.; Yu, W.; Chen, W. Sedimentary records of seismic events in a lacustrine basin of continental depression: A case study of the Triassic Yanchang Formation in the Ordos Basin, Northern China. *J. Asian Earth Sci.* **2022**, *228*, 105128. [[CrossRef](#)]
62. Fedo, C.M.; Sircombe, K.N.; Rainbird, R.H. Detrital Zircon Analysis of the Sedimentary Record. *Rev. Mineral. Geochem.* **2003**, *53*, 277–303. [[CrossRef](#)]
63. Fonneland, H.; Lien, T.; Martinsen, O.; Pedersen, R.; Košler, J. Detrital zircon ages: A key to understanding the deposition of deep marine sandstones in the Norwegian Sea. *Sediment. Geol.* **2004**, *164*, 147–159. [[CrossRef](#)]
64. Hu, Z.; Zhang, W.; Liu, Y.; Gao, S.; Li, M.; Zong, K.; Chen, H.; Hu, S. “Wave” Signal-Smoothing and Mercury-Removing Device for Laser Ablation Quadrupole and Multiple Collector ICPMS Analysis: Application to Lead Isotope Analysis. *Anal. Chem.* **2015**, *87*, 1152–1157. [[CrossRef](#)] [[PubMed](#)]
65. Wiedenbeck, M.; Allé, P.; Corfu, F.; Griffin, W.L.; Meier, M.; Oberli, F.; Quadt, A.; Roddick, J.C.; Spiegel, W. Three natural zircon standards for U-Th-Pb, Lu-Hf, trace element, and REE analyses. *Geostand. Geoanal. Res.* **1995**, *19*, 1–23. [[CrossRef](#)]
66. Pearce, N.; Perkins, W.; Westgate, J.; Gorton, M.P.; Jackson, S.; Neal, C.; Chenery, S. A compilation of new and published major and trace element data for NIST SRM 610 and NIST SRM 612 glass reference materials. *Geostand. Newslett.* **1997**, *21*, 115–144. [[CrossRef](#)]
67. Liu, Y.; Hu, Z.; Gao, S.; Günther, D.; Xu, J.; Gao, C.; Chen, H. In situ analysis of major and trace elements of anhydrous minerals by LA-ICP-MS without applying an internal standard. *Chem. Geol.* **2008**, *257*, 34–43. [[CrossRef](#)]
68. Liu, Y.; Hu, Z.; Zong, K.; Gao, C.; Gao, S.; Xu, J.; Chen, H. Reappraisal and refinement of zircon U-Pb isotope and trace element analyses by LA-ICP-MS. *Chin. Sci. Bull.* **2010**, *55*, 1535–1546. [[CrossRef](#)]
69. Barosh, P.J. Paleozoic Rifting in New England, New Brunswick and Nova Scotia, U.S.A. and Canada. In *Basement Tectonics 10. Proceedings of the 10th International Conferences on Basement Tectonics, Duluth, MN, USA, 1–11 August 1992*; Ojakangas, R.W., Dickas, A.B., Green, J.C., Eds.; Springer: Dordrecht, Germany, 1995; Volume 4, p. 4. [[CrossRef](#)]

70. Landing, E.; Webster, M. Iapetan rift–passive margin transition in NE Laurentia and eustatic control on continental slope oxygenation, Taconic slate colors, and Early Paleozoic climate. In *Guidebook to Field Trips in New York, Vermont, and Massachusetts: 110th New England Intercollegiate Geological Conference and 90th New York Geological Association, Lake George, NY, USA, 12–14 October 2018*; pp. A5–A45. Available online: <https://www.nysm.nysed.gov/staff-publications/iapetan-rift%E2%80%92passive-margin-transition-ne-laurentia-and-eusta> (accessed on 7 March 2024).
71. Tobin, R.C.; Schwarzer, D. Effects of sandstone provenance on reservoir quality preservation in the deep subsurface: Experimental modelling of deep-water sand in the Gulf of Mexico. *Geol. Soc. Lond. Spec. Publ.* **2014**, *386*, 27–47. [[CrossRef](#)]
72. Gawthorpe, R.L.; Leeder, M.R. Tectono-sedimentary evolution of active extensional basins. *Basin Res.* **2000**, *12*, 195–218. [[CrossRef](#)]
73. Wang, R.J.; Wang, S.J.; Xian, B.; Zhu, S.B.; Fan, Q.H.; Shan, C.A.; Shao, J.B.; Wang, H.; Zhang, R.J.; Ye, Z.C. Sedimentary microfacies and configuration of skeleton sand bodies in the third member of Bashijiqike Formation in northern Kuqa Depression, Tarim Basin. *Nat. Gas Geosci.* **2023**, *34*, 1681–1695. (In Chinese with English Abstract)
74. DeGraaff-Surpless, K.; Graham, S.A.; Wooden, J.L.; McWilliams, M.O. Detrital zircon provenance analysis of the Great Valley Group, California: Evolution of an arc-forearc system. *Geol. Soc. Am. Bull.* **2003**, *115*, 639. [[CrossRef](#)]
75. Link, P.K.; Fanning, C.M.; Beranek, L.P. Reliability and Longitudinal Change of Detrital-Zircon Age Spectra in the Snake River System, Idaho and Wyoming: An Example of Reproducing the Bumpy Barcode. *Sediment. Geol.* **2005**, *182*, 101–142. [[CrossRef](#)]
76. Liu, J.H.; Wu, Z.X.; Yu, S.; Jia, D.H. Paleocene trace element geochemistry and its geological significance in Lishui sag. *China Offshore Oil Gas* **2005**, *17*, 8–11. (In Chinese with English Abstract) [[CrossRef](#)]
77. Chen, G.J.; Li, C.; Liang, J.S.; Wang, Q.; LV, C.F.; Zhang, J.W.; Du, G.C.; Tian, B. Sedimentary Facies of Mingyuefeng Formation in Oujiang Sag, East China Sea Basin. *Nat. Gas Geosci.* **2011**, *22*, 10. (In Chinese with English Abstract)
78. Deng, Y.; Xu, C.; Gao, S.; Fu, Q.; Li, Y. Evolved Late Mesozoic continental arc: Constraints of detrital zircons from the western East China Sea. *Int. Geol. Rev.* **2023**. [[CrossRef](#)]
79. North, C.P.; Davidson, S.K. Unconfined alluvial flow processes: Recognition and interpretation of their deposits, and the significance for palaeogeographic reconstruction. *Earth-Sci. Rev.* **2012**, *111*, 199–223. [[CrossRef](#)]
80. Raiverman, V. *Foreland Sedimentation in Himalayan Tectonic Regime: A Relook at the Orogenic Process*; Bishen Singh Mahendra Pal Singh Publishers: Dehradun, India, 2002.
81. Singh, S.; Awasthi, A.; Khanna, Y.; Kumari, A.; Singh, B.; Kumar, A.; Popli, C. Sediment colour as recorder of climate and tectonics: Cenozoic continental red beds of the Himalayan foreland basin in NW India. *Catena* **2021**, *203*, 105298. [[CrossRef](#)]

**Disclaimer/Publisher’s Note:** The statements, opinions and data contained in all publications are solely those of the individual author(s) and contributor(s) and not of MDPI and/or the editor(s). MDPI and/or the editor(s) disclaim responsibility for any injury to people or property resulting from any ideas, methods, instructions or products referred to in the content.